

Rods of Neutron Scattering Intensity in $\text{Yb}_2\text{Ti}_2\text{O}_7$: Compelling Evidence for Significant Anisotropic Exchange in a Magnetic Pyrochlore Oxide

Jordan D. Thompson,¹ Paul A. McClarty,¹ Henrik M. Rønnow,²
Louis P. Regnault,³ Andreas Sorge,^{4,5} and Michel J. P. Gingras^{1,5,6}

¹*Department of Physics and Astronomy, University of Waterloo, Waterloo, ON, Canada, N2L 3G1*

²*Laboratory for Quantum Magnetism, École Polytechnique Fédérale de Lausanne (EPFL), CH-1015 Lausanne, Switzerland*

³*CEA-Grenoble, INAC-SPSMS-MDN, 17 rue des Marthyrs, 38054 Grenoble, cedex 9, France*

⁴*Network Dynamics Group, MPI for Dynamics and Self-Organization, Bunsenstr. 10, 37073 Göttingen, Germany*

⁵*Department of Physics and Astronomy, University of Canterbury, Private Bag 4800, Christchurch, New Zealand*

⁶*Canadian Institute for Advanced Research, 180 Dundas Street West, Toronto, Ontario M5G 1Z8, Canada*

(Dated: March 8, 2019)

The paramagnetic correlations in the exotic pyrochlore material $\text{Yb}_2\text{Ti}_2\text{O}_7$ have been investigated via neutron scattering revealing, among other features, a [111] rod of scattering intensity. Assuming interactions between the Yb^{3+} ions composed of all symmetry-allowed nearest neighbor anisotropic exchange interactions and long-range dipole-dipole interactions, we find a set of interactions that provide an excellent fit to the data by computing the diffuse scattering using a random phase approximation. Our results provide compelling evidence for significant anisotropic exchange interactions in an insulating magnetic pyrochlore oxide. In addition, by computing real space correlations, we find that the [111] rod of scattering is consistent with weaker correlations between kagome planes than within these planes in a cubic material *without* structural distortion.

Magnetic materials that comprise antiferromagnetically coupled spins residing on sites of regular lattices made of interconnected triangles or tetrahedra exhibit geometric frustration, meaning that the simultaneous minimization of interactions between magnetic moments is impossible. Experimental and theoretical research over the past twenty years has shown that frustrated magnetic systems are prone to exhibit novel and intriguing collective thermodynamic phenomena [1].

Among frustrated three dimensional systems, the $A_2B_2O_7$ pyrochlores have attracted much attention [2]. In these compounds, A is a trivalent rare earth ion (Ho, Tb, Gd, Yb) or yttrium (Y) and B is a tetravalent transition metal ion (Ti, Sn, Mo). The A and B ions reside on two distinct (pyrochlore) lattices of corner-sharing tetrahedra. A celebrated example of frustration on this lattice is a model of Heisenberg spins interacting via an isotropic antiferromagnetic nearest neighbor exchange Hamiltonian. Remarkably, classical [3] and quantum [4] variants of this model fail to develop conventional long range order (LRO) down to zero temperature. In real pyrochlore compounds, however, there typically exist material-specific interactions of various kinds, which may be frustrated individually, and which most often compete with each other, resulting in the richness of phenomena observed in these systems [2]. Examples include spin liquid [5], spin glass [6], and spin ice [7] states as well as LRO with persistent low-temperature spin dynamics [8, 9]. In this article, we consider the $\text{Yb}_2\text{Ti}_2\text{O}_7$ pyrochlore which exhibits some unique and unusual features of its own and which have heretofore remained unexplained.

$\text{Yb}_2\text{Ti}_2\text{O}_7$ has an ferromagnetic character, with a Curie-Weiss temperature $\theta_{\text{CW}} = +0.65 \pm 0.15$ K [10, 11] and with the $\text{Yb}^{3+} \sim 3 \mu_{\text{B}}$ magnetic moments predom-

inantly lying perpendicular to the local [111] cubic unit cell diagonals, hence making this system the only known local [111] XY pyrochlore ferromagnet [2]. Magnetic specific heat (C_m) measurements reveal a sharp first order transition at $T_c \approx 240$ mK [12], suggesting the onset of LRO. While a single crystal elastic neutron scattering (NS) study suggested ferromagnetic order below T_c [13], a subsequent polarized NS study [14] did not confirm such ordering. Furthermore, powder NS shows no LRO down to 110 mK [15] and very recent NS on a single crystal sample has not found any sign of LRO in a broad region of the (hkk) scattering plane at 30 mK [16]. The $T_c \approx 240$ mK transition seen in C_m has therefore not been matched with the observation of conventional (dipolar magnetic) LRO to date. In addition, Mössbauer spectroscopy and muon spin relaxation (muSR) measurements find a rapid decrease of the Yb^{3+} magnetic moments fluctuation rate ν upon approaching T_c from above, with muSR revealing a temperature-independent ν (i.e. persistent spin dynamics) from T_c down to 40 mK, the lowest temperature considered [15]. Considering all these results together, one may ask whether the 240 mK transition in $\text{Yb}_2\text{Ti}_2\text{O}_7$ may be another rare and interesting example of hidden (non-dipolar) order [17]. Another intriguing possibility [15] is that the 240 mK first order transition takes place between a “spin gas” (paramagnetic) state and a spin liquid without any symmetry breaking.

A very interesting feature of the magnetic correlations in $\text{Yb}_2\text{Ti}_2\text{O}_7$ found at temperatures $T_c < T \lesssim 10$ K are rods of NS intensity along the [111] directions [9, 16]. At first sight, the presence of such rods signals an anisotropy in the magnetic correlations that might originate from a structural transition at $T \gtrsim 10$ K or from *intrinsically* stronger correlations within the kagome planes perpen-

dicular to the four [111] directions that form the undistorted pyrochlore structure [2] compared to correlations perpendicular to these planes [16] – hence making this system a “spin liquid crystal” of sorts.

Here, we report results from diffuse NS measurements on $\text{Yb}_2\text{Ti}_2\text{O}_7$ in a temperature range above $\theta_{\text{CW}} > T_c$. By numerically annealing a set of exchange couplings to maximize the agreement between the experimental results and the NS computed within a random phase approximation (RPA), we determine a spin Hamiltonian, \mathcal{H} , that captures the main features of the observed paramagnetic NS pattern and reveals that significant spin exchange anisotropy exists in this insulating pyrochlore oxide. There have been recent claims of evidence for anisotropic exchange in $\text{Yb}_2\text{Ti}_2\text{O}_7$ [18, 19] and other $A_2B_2O_7$ pyrochlores [18, 20]. Unfortunately, due to the limited information contained in the local magnetic susceptibility analyzed in Refs. [18–20], the nature and symmetry of the putative microscopic exchange remains hidden. Here, thanks to the highly structured spin correlation functions in $\text{Yb}_2\text{Ti}_2\text{O}_7$, we are able to obtain highly compelling evidence for anisotropic exchange. From the spin structure factor, we compute the spin-spin correlations along different crystallographic directions, finding that, while the correlations are anisotropic, the correlation lengths themselves do not distinguish between correlations parallel and perpendicular to the kagome planes.

The NS cross-section was measured on the D23 diffractometer at the Institut Laue Langevin, France. A single crystal rod was aligned with [h00] and [0kk] in the scattering plane, hence providing access to all principal symmetry directions of the cubic crystal structure. With incident neutron energy of 14.7 meV, significantly larger than any characteristic interaction scale in the system, and counting all final energies, the measured intensity is proportional to the spatial Fourier transform of the instantaneous correlation function $S(q) = \int S(q, \omega) d\omega$.

Figures 1(a,b) show experimental NS data for $\text{Yb}_2\text{Ti}_2\text{O}_7$ at $T = 9.1$ K and $T = 1.4$ K in the (hkk) plane respectively. The intense Bragg peaks at integer reciprocal lattice positions were removed from the data to make visible significant structure in the diffuse magnetic scattering. Fig. 1a shows the NS map at $T = 9.1$ K. The magnetic correlations weaken with increasing temperature. Indeed, most of the features present at $T = 1.4$ K (Fig. 1b) are absent at 9.1 K, with only a weakened rod of scattering (RoS) along [111] and a feature in the upper right corner at 3.5, 2.25, 2.25 remaining. Fig. 1b shows the NS map at $T = 1.4$ K, where the most interesting feature is the RoS along the [111] direction [9, 16]. Fig. 1b exhibits other features of interest such as a weaker RoS going from 400 to 222 and intensity around the point 022. The intensity of the feature centered on 3.5, 2.25, 2.25 does not change with temperature (Fig. 1f) indicating that it is not magnetic in origin and can therefore be omitted from further consideration.

To explain the NS pattern, we propose a Hamiltonian, $\mathcal{H} = \mathcal{H}_{\text{cf}} + \mathcal{H}_{\text{int}}$, that includes a crystal field (CF) part, \mathcal{H}_{cf} , and spin-spin interactions, $\mathcal{H}_{\text{int}} = \mathcal{H}_{\text{dip}} + \mathcal{H}_{\text{ex}}$. The form of \mathcal{H}_{cf} is fixed by the symmetry of the Yb^{3+} environment. The two sets of CF parameters that we use have been determined in Refs. [15, 18]. The magnetic Yb^{3+} ion has electronic configuration $^2F_{7/2}$, hence $J = 7/2$ and Landé factor $g_J = 8/7$. The nearest neighbor distance between Yb^{3+} ions is $r_{\text{nn}} = (a/4)\sqrt{2}$, where $a = 10.026$ Å is the size of the conventional cubic unit cell [14]. This fixes the strength of the coupling $D = \frac{\mu_0(g_J\mu_B)^2}{4\pi r_{\text{nn}}^3} \approx 0.01848$ K of the long-range magnetostatic dipolar interaction, $\mathcal{H}_{\text{dip}} = \sum_{i>j;a,b} \frac{D(r_{\text{nn}})^3}{|\mathbf{R}_{ij}^{ab}|^3} (\mathbf{J}_i^a \cdot \mathbf{J}_j^b - 3(\mathbf{J}_i^a \cdot \hat{\mathbf{R}}_{ij}^{ab})(\mathbf{J}_j^b \cdot \hat{\mathbf{R}}_{ij}^{ab}))$. We also consider \mathcal{H}_{ex} which contains all nearest neighbor exchange interactions, \mathcal{J}_e , that respect lattice symmetries. There are four such nearest neighbor interactions [21]: $\mathcal{H}_{\text{Ising}} = -\mathcal{J}_{\text{Ising}} \sum_{\langle i,j \rangle; a,b} (\mathbf{J}_i^a \cdot \hat{\mathbf{z}}^a)(\mathbf{J}_j^b \cdot \hat{\mathbf{z}}^b)$, which couples the local [111] $\hat{\mathbf{z}}$ components of \mathbf{J} , $\mathcal{H}_{\text{iso}} = -\mathcal{J}_{\text{iso}} \sum_{\langle i,j \rangle; a,b} \mathbf{J}_i^a \cdot \mathbf{J}_j^b$, the standard isotropic exchange, $\mathcal{H}_{\text{pd}} = -\mathcal{J}_{\text{pd}} \sum_{\langle i,j \rangle; a,b} (\mathbf{J}_i^a \cdot \mathbf{J}_j^b - 3(\mathbf{J}_i^a \cdot \hat{\mathbf{R}}_{ij}^{ab})(\mathbf{J}_j^b \cdot \hat{\mathbf{R}}_{ij}^{ab}))$, a pseudo-dipolar interaction of exchange origin and not part of \mathcal{H}_{dip} and, finally, $\mathcal{H}_{\text{DM}} = -\mathcal{J}_{\text{DM}} \sum_{\langle i,j \rangle; a,b} \boldsymbol{\Omega}_{\text{DM}}^{a,b} \cdot (\mathbf{J}_i^a \times \mathbf{J}_j^b)$, the Dzyaloshinskii-Moriya (DM) interaction [22]. In all of these terms, \mathbf{J}_i^a denotes the angular momentum of the Yb^{3+} located at lattice \mathbf{R}_i^a (FCC lattice site i , and tetrahedral sub-lattice site a) $\hat{\mathbf{R}}_{ij}^{ab}$ a unit vector directed along $\mathbf{R}_j^b - \mathbf{R}_i^a$.

We use \mathcal{H} to compute the diffuse NS pattern by employing the RPA [23, 24]. The RPA, which uses the bare single-ion anisotropy as the non-interacting reference susceptibility, is justified here for two important reasons. Firstly, \mathcal{H}_{ex} and \mathcal{H}_{dip} are very weak compared to the large (~ 700 K) energy gap between the ground and first excited CF doublets [11] and, unlike in $\text{Tb}_2\text{Ti}_2\text{O}_7$ [25], there is negligible interaction-induced admixing between the ground and first excited CF doublets. Secondly, the correlations used to calculate the NS are at a temperature of about twice the Curie-Weiss temperature with the system still in the paramagnetic regime, where RPA is reasonably valid. We first compute the single ion susceptibility, $\chi^{(0)}$, from \mathcal{H}_{cf} :

$$\chi_a^{(0),\alpha\beta}(\omega) = \sum_{\mu,\nu}^{E_\mu \neq E_\nu} \frac{M_{\nu\mu,a}^\alpha M_{\mu\nu,a}^\beta}{E_\mu - E_\nu - \hbar(\omega + i0^+)} (n_\nu - n_\mu) + \frac{\delta(\omega)}{k_B T} \sum_{\mu,\nu}^{E_\mu = E_\nu} M_{\nu\mu,a}^\alpha M_{\mu\nu,a}^\beta n_\nu, \quad (1)$$

where n_ν is the thermal occupation fraction for CF state ν of energy E_ν . The $M_{\nu\mu,a}^\alpha$ matrix elements for the single-ion states are given by $M_{\nu\mu,a}^\alpha = \sum_{\bar{\alpha}} \langle \nu | \mathbf{J}^{\bar{\alpha}} | \mu \rangle u_{\bar{\alpha},a}^\alpha$, where $u_{\bar{\alpha},a}^\alpha$ is the rotation matrix from the local ($\bar{\alpha}$) frame defined on sublattice a to the global (α) frame. The operator $\mathbf{J}^{\bar{\alpha}}$ acts on the CF states defined in the local $\bar{\alpha}$ quantization frame. The CF wavefunctions

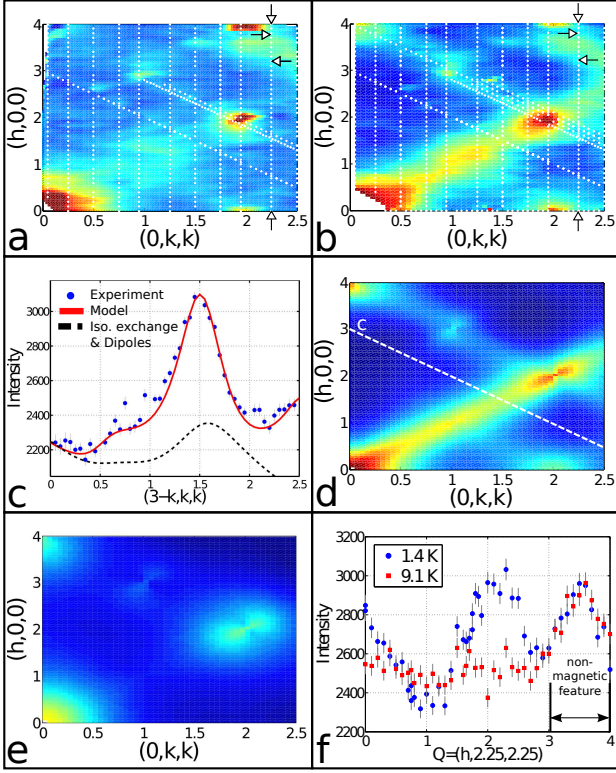


FIG. 1: (Color online) Neutron scattering (NS) maps in the (h,k,k) plane. (a) and (b) show experimental data at 9.1 K and 1.4 K, respectively. In (b) a rod of scattering (RoS) along $[111]$ can be clearly seen, while in (a) the RoS is not strong. (c) shows a comparison between experimental data and the computed NS intensity at 1.4 K along $[3-k, k, k]$ for both isotropic exchange and the full model. (d) shows computed NS using the Hamiltonian \mathcal{H} (see text), at $T = 1.4$ K. (e) shows the calculated NS using \mathcal{H} with only isotropic exchange determined from fitting θ_{CW} and long-range dipolar interactions at $T = 1.4$ K. (f) shows experimental neutron scattering at 1.4 K and 9.1 K along $[h, 2.25, 2.25]$ showing that the feature between $h = 3$ and $h = 4$ does not change in intensity with temperature. The white arrows in (a) and (b) indicate the range $h \in [3, 4]$ in $[h, 2.25, 2.25]$ in panel (f).

$|\nu\rangle$, at sublattice site a , are obtained by diagonalizing \mathcal{H}_{cf} [15, 18]. The interacting RPA susceptibility, $\chi(\mathbf{q}, \omega)$, is then $\chi_{ab}^{\alpha\beta}(\mathbf{q}, \omega) + \sum_{\gamma, \delta; c} \chi_a^{0, \alpha\gamma}(\omega) \mathcal{J}_{ac}^{\gamma\delta}(\mathbf{q}) \chi_{cb}^{\delta\beta}(\mathbf{q}, \omega) = \delta_{ab} \chi_a^{0, \alpha\beta}(\omega)$, where $\mathcal{J}(\mathbf{q})$ is the Fourier transformation of the interaction matrix $\mathcal{J}(i, j)$ for Hamiltonian $\mathcal{H}_{int} = -(1/2) \sum_{i, j; a, b; \alpha, \beta} J_{i, a}^{\alpha} \mathcal{J}_{ab}^{\alpha\beta}(i, j) J_{j, b}^{\beta}$. The infinite lattice sum of the dipolar interaction is computed using Ewald summation [26]. We solve for $\chi_{ab}^{\alpha\beta}(\mathbf{q}, \omega)$ numerically. Finally, the NS function, $S(\mathbf{q}, \omega)$, is given by [23, 24]

$$S(\mathbf{q}, \omega) \propto \frac{|f(\mathbf{Q})|^2}{k_B T} \sum_{\alpha, \beta} \sum_{a, b} (\delta_{\alpha\beta} - \hat{Q}_\alpha \hat{Q}_\beta) \quad (2)$$

$$\times \exp(-i(\mathbf{r}^a - \mathbf{r}^b) \cdot \mathbf{G}) \operatorname{Re} \left(\chi_{ab}^{\alpha\beta}(\mathbf{q}, \omega) \right)$$

where $f(\mathbf{Q})$ is the magnetic form factor for the Yb^{3+} ion [27]. $\mathbf{Q} = \mathbf{q} + \mathbf{G}$ is the scattering wave vector where \mathbf{q} is

a wave vector inside the first Brillouin zone, and \mathbf{G} is an FCC reciprocal lattice vector. \mathbf{r}^a and \mathbf{r}^b are basis vectors for the tetrahedral sublattice [26].

The fit to the experimental data was performed by computing the RPA scattering intensity along the measured lines in \mathbf{Q} space (dashed lines in Fig. 1b). The computed intensities were rescaled to the experimental count rate using the relation $S'(\mathbf{q}) = c_0 S(\mathbf{q}) + c_1 + c_2 |\mathbf{Q}|$ [28], where the parameters c_0 , c_1 , and c_2 are the same for all \mathbf{Q} points. There are therefore seven adjustable parameters in total with the four exchange couplings, \mathcal{J}_e and the three c_n fitting parameters. The variance between the measured and calculated neutron data, with a contribution to the variance from fitting θ_{CW} as well, was minimized using a simulated annealing algorithm [29]. As a first step, for simplicity and computational speed, we make a static approximation to $S(\mathbf{q}, \omega)$, ($\omega = 0$ and $\delta(\omega) \rightarrow 1$ in Eq. (1) [30]). For the set of parameters obtained from the annealing and the static approximation, we carried out a more rigorous energy integrated calculation of the full dynamical scattering function, $S(\mathbf{q}, \omega)$. Doing so, we obtain a very similar intensity map, but not quantitatively identical to the one calculated within the static approximation. Also, because the RPA NS intensity was calculated at $T = 1.4$ K $\sim 2\theta_{CW}$, we expect the fitted anisotropic exchange coupling to be affected by a slight thermal renormalization factor of order $1/(T - \theta_{CW})^2 \approx 25\%$, the leading correction in a high temperature expansion of $\chi(\mathbf{q})$, compared to that of the RPA approximation of $\chi(\mathbf{q})$. That said, the present calculation is suitable to reach the main conclusion of this work: that significant anisotropic exchange couplings \mathcal{J}_e are necessary to account for the structure of the NS pattern of $\text{Yb}_2\text{Ti}_2\text{O}_7$.

Fig. 1d shows the RPA NS pattern in the (hkk) plane at 1.4 K obtained from simulated annealing fits to the experimental neutron scattering map of Fig. 1b. The model data in Fig. 1d is obtained using the CF parameters from Ref. [15] and from an \mathcal{H}_{ex} with $\mathcal{J}_{sing} = 0.81$ K, $\mathcal{J}_{iso} = 0.22$ K, $\mathcal{J}_{pd} = -0.29$ K, and $\mathcal{J}_{DM} = -0.27$ K. The calculated intensity matches the experimental data (Fig. 1b) well, providing strong evidence that our model \mathcal{H}_{ex} contains the correct interactions for $\text{Yb}_2\text{Ti}_2\text{O}_7$. A cut along $[3-k, k, k]$ (Fig. 1c) emphasizes the quantitative agreement between the computed and experimental NS intensities. A similar quality of fit was obtained for other line scans (dashed lines in Fig. 1b). We also carried out the fitting procedure using CF parameters for \mathcal{H}_{cf} taken from Ref. [18] and found that the exchange couplings do not change significantly. Fig. 1e and the dashed (black) line in Fig. 1c show the NS intensity calculated for a model \mathcal{H}_{int} with only long-range dipolar and isotropic exchange interactions ($\mathcal{J}_{sing} = \mathcal{J}_{pd} = \mathcal{J}_{DM} = 0$) with $\mathcal{J}_{iso} = 0.06$ K, determined by fitting θ_{CW} , and refitted c_n 's. Clearly this model and the resulting NS pattern do not describe the experimental data (Fig. 1b) well at all.

To rationalize the direct space origin of the RoS, we computed the spin-spin correlation function from the reciprocal space RPA susceptibility $\langle J_a^\alpha(\mathbf{r}) J_b^\beta(\mathbf{0}) \rangle = k_B T \int \chi_{ab}^{\alpha\beta}(\mathbf{q}) \exp(\mathbf{q} \cdot \mathbf{r}) d\mathbf{q}$ where $\mathbf{r} = \mathbf{R}_j^b - \mathbf{R}_i^a$. The integral was performed numerically over the first Brillouin zone. We considered the isotropic real space correlations (by summing over all directions in spin space) $S(\mathbf{r}) \equiv \sum_\alpha \langle J_a^\alpha(\mathbf{r}) J_b^\alpha(\mathbf{0}) \rangle$ and also $S_\perp(\mathbf{r}) \equiv k_B T \int (\delta_{\alpha\beta} - \hat{q}_\alpha \hat{q}_\beta) \chi_{ab}^{\alpha\beta}(\mathbf{q}) \exp(\mathbf{q} \cdot \mathbf{r}) d\mathbf{q}$ which computes the real space correlations one would obtain purely from the NS. Fig. 2 shows $S(\mathbf{r})$ and $S_\perp(\mathbf{r})$ for \mathbf{r} taken along the $[111]$ direction and $[0\bar{1}1]$, $[1\bar{2}1]$ perpendicular to $[111]$. $S(\mathbf{r})$ and $S_\perp(\mathbf{r})$ are similar so we discuss both together. The correlation lengths from these three directions were extracted assuming exponential decay and found not to differ greatly within our margin of error. However, the $[0\bar{1}1]$ correlations are larger than those for the other two directions indicating some degree of spontaneous decoupling of the kagome planes, albeit with quasi-isotropic correlation lengths. Since the $[0\bar{1}1]$ directions lie within two kagome planes and the $[1\bar{2}1]$ directions in only one kagome plane, truly two dimensional correlations would be expected to lead to the splitting $S(\mathbf{r})_{[0\bar{1}1]} > S(\mathbf{r})_{[1\bar{2}1]} > S(\mathbf{r})_{[111]}$. This is not borne out by our results - the similarity of $S(\mathbf{r})$ for the $[1\bar{2}1]$ and $[111]$ directions indicates that the correlations are strongest along chains of spins. Whereas the $(h\bar{h}k)$ plane of NS intensity, considered on its own, suggests that the correlations are quasi two-dimensional with a weak decoupling of the kagome planes [16], the real space spin-spin correlators obtained from our model do not support this picture.

From the determined \mathcal{H}_{ex} , RPA predicts a second order phase transition to a ferromagnetic phase (ordering wavevector $\mathbf{q} = 0$) at a critical temperature $T_c^{\text{RPA}} \approx 1.2$ K. We expect thermal and quantum fluctuations to significantly renormalize this T_c value and work to investigate these effects is in progress. In the context of this finding, it would be most useful to revisit the low-temperature phase of $\text{Yb}_2\text{Ti}_2\text{O}_7$ [13–16] and, in particular, systematically compare the behavior of single crystals [13, 14, 16] with powder samples [12, 15].

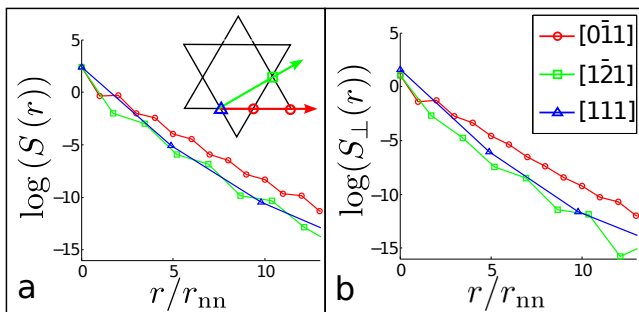


FIG. 2: (Color online) Real space spin-spin correlation functions (a) $S(\mathbf{r})$ and (b) $S_\perp(\mathbf{r})$ (see text) computed at $T = 1.4$ K using the anisotropic exchange model and plotted along various crystallographic directions.

In summary, we have presented diffuse neutron scattering (NS) maps of $\text{Yb}_2\text{Ti}_2\text{O}_7$ in its paramagnetic regime finding rods of scattering in the $\langle 111 \rangle$ directions. By fitting this data to NS computed from a candidate microscopic Hamiltonian, we found a set of couplings that reproduce the main features of this NS pattern. The Hamiltonian includes, as an essential component, sizeable anisotropic exchange interactions. This suggests that anisotropic exchange might be important in other $A_2B_2O_7$ rare earth magnets [18, 20]. We find that the rods of scattering occur without any symmetry breaking from, for example, a structural phase transition. We anticipate that our results will allow for a greater understanding of the nature of the phase transition at 240 mK and of the low temperature phase of $\text{Yb}_2\text{Ti}_2\text{O}_7$.

We thank Y.-J. Kao for useful discussions and contributions at the earliest stage of this project. We acknowledge useful discussions with B. Gaulin, K. Ross and J. Ruff. This work was funded by the NSERC of Canada and the CRC Program (M.G., Tier 1).

-
- [1] H.T. Diep, *Frustrated Spin Systems*, (World Scientific Publishing Co. Pte. Ltd., 2004, Hackensack).
 - [2] J. S. Gardner, M. J. P. Gingras, and J. E. Greedan, *Rev. Mod. Phys.* **82**, 53 (2010).
 - [3] R. Moessner and J. T. Chalker, *Phys. Rev. Lett.* **80**, 2929 (1998).
 - [4] B. Canals and C. Lacroix, *Phys. Rev. Lett.* **80**, 2933 (1998).
 - [5] J. S. Gardner *et al.*, *Phys. Rev. Lett.* **82**, 1012 (1999).
 - [6] M. J. P. Gingras *et al.*, *Phys. Rev. Lett.* **78**, 947 (1997).
 - [7] S. T. Bramwell and M. J. P. Gingras, *Science* **294**, 1495 (2001).
 - [8] Y. Chapuis *et al.*, *Physica B* **404** 686 (2009).
 - [9] P. Bonville *et al.*, *Hyperfine Interactions* **156**, 103 (2004); *ibid.* arXiv:cond-mat/0306470;
 - [10] S. T. Bramwell *et al.*, *J. Phys.: Condens. Matter* **12** 483 (2000).
 - [11] J. A. Hodges *et al.*, *J. Phys. Condens. Matter* **13**, 9301 (2001).
 - [12] H. W. J. Blöte, R. F. Wierlinga, and W. J. Huiskamp, *Physica (Amsterdam)* **43**, 549 (1969).
 - [13] Y. Yasui *et al.*, *J. Phys. Soc. Jpn.* **72**, 3014 (2003).
 - [14] J. S. Gardner *et al.*, *Phys. Rev. B* **70**, 180404(R) (2004).
 - [15] J. A. Hodges *et al.*, *Phys. Rev. Lett.* **88**, 077204 (2002).
 - [16] K. A. Ross *et al.*, *Phys. Rev. Lett.* **103**, 227202 (2009).
 - [17] P. Santini *et al.*, *Rev. Mod. Phys.* **81**, 807 (2009).
 - [18] H. B. Cao *et al.*, *Phys. Rev. Lett.* **103**, 056402 (2009).
 - [19] H. B. Cao *et al.*, *J. Phys.: Condens. Matter* **21**, 492202 (2009).
 - [20] B. Z. Malkin *et al.*, *J. Phys.: Condens. Matter* **22**, 276003 (2010).
 - [21] P. A. McClarty *et al.*, *J. Phys.: Conference Series* **145**, 012032 (2009).
 - [22] M. Elhajal *et al.* *Phys. Rev. B* **71**, 094420 (2005).
 - [23] J. Jensen and A. R. Mackintosh, *Rare Earth Magnetism*, (Clarendon Press, 1991, Oxf ord).
 - [24] Y. -J. Kao *et al.*, *Phys. Rev. B* **68**, 172407 (2003).

- [25] H. R. Molavian, M. J. P. Gingras and B. Canals, Phys. Rev. Lett. **98**, 157204 (2007).
- [26] M. Enjalran and M. J. P. Gingras, Phys. Rev. B **70**, 174426 (2004).
- [27] P. J. Brown in *International Tables for Crystallography*, Vol. C, Ed. A. J. C. Wilson Kluwer Academic Publishers, pages 393 and 395, (1992).
- [28] T. Yavors'kii *et al.*, Phys. Rev. Lett. **101**, 037204 (2008).
- [29] W. H. Press, S. A. Teukolsky, W. T. Vetterling, and B. P. Flannery *Numerical Recipes: The Art of Scientific Computing*, (Cambridge University Press, 2007, Cambridge).
- [30] S. W. Lovesey, *Theory of Neutron Scattering from Condensed Matter* (Clarendon Press, 1984, Oxford).